Chemical Science

ROYAL SOCIETY OF CHEMISTRY

EDGE ARTICLE

View Article Online
View Journal | View Issue



Cite this: *Chem. Sci.*, 2024, **15**, 16582

All publication charges for this article have been paid for by the Royal Society of Chemistry



# Efficient DNP at high fields and fast MAS with antenna-sensitized dinitroxides†

Lorenzo Niccoli,‡[abcd] Gilles Casano,‡[e] Georges Menzildjian,‡[a] Maxim Yulikov,[f] Thomas Robinson,[a] Salah-Eddine Akrial,[a] Zhuoran Wang,[a] Christian Reiter,[g] Armin Purea,[g] Didier Siri,[e] Amrit Venkatesh,[hi] Lyndon Emsley,[h] David Gajan,[a] Moreno Lelli,*[bcd] Olivier Ouari*[e] and Anne Lesage*[a]

Received 5th July 2024
Accepted 10th September 2024

DOI: 10.1039/d4sc04473h

rsc.li/chemical-science

Dynamic Nuclear Polarization (DNP) can significantly enhance the sensitivity of solid-state NMR. In DNP, microwave irradiation induces polarization transfer from unpaired electron spins to $^{1}$H nuclear spins *via* hyperfine couplings and spin-diffusion. The structure of the polarizing agents that host the electron spins is key for DNP efficiency. Currently, only a handful of structures perform well at very high magnetic fields (≥18.8 T), and enhancements are significantly lower than those obtained at lower fields. Here, we introduce a new series of water-soluble nitroxide biradicals with a scaffold augmented by dihydroxypropyl antenna chains that perform significantly better than previous dinitroxides at 18.8 T. The new radical M-TinyPol(OH)$_4$ yields enhancement factors of ∼220 at 18.8 T and 60 kHz MAS, which is a nearly factor 2 larger than for the previous best performing dinitroxides. The performance is understood through $^{2}$H ESEEM measurements to probe solvent accessibility, supported by Molecular Dynamics simulations, and by experiments on deuterated samples. We find that the deuterated glycerol molecules in the matrix are located mainly in the second solvation shell of the NO bond, limiting access for protonated water molecules, and restricting spin diffusion pathways. This provides a rational understanding of why the dihydroxypropyl chains present in the best-performing structures are essential to deliver the polarization to the bulk solution.

## Introduction

Solid-state magic angle spinning (MAS) nuclear magnetic resonance (NMR) spectroscopy is a powerful analytical technique that can provide atomic-level structural information on a broad range of solid substrates.[1] Despite its high versatility, MAS NMR inherently lacks sensitivity due to low nuclear spin polarization at thermal equilibrium. To remediate this limitation significant developments have been made with microwave-driven dynamic nuclear polarization (DNP) in the last decades.[2–6] DNP routinely yields ∼100-fold NMR signal amplification at cryogenic temperatures, and DNP enhanced solid-state NMR has already enabled many challenging new applications, overcoming the limitations of conventional MAS NMR spectroscopy, in research fields as diverse as nanomaterials, batteries, pharmaceuticals, polymers, supported catalysts, biomaterials, *in vitro* and *in cell* biomolecules.[7–25] This boost in sensitivity is typically achieved by doping the substrate of interest with a polarizing agent (PA) containing unpaired electron spins, which transfer their significantly larger spin polarization to the surrounding nuclear spins under microwave irradiation.

Today, a large library of PAs with different molecular scaffolds have been introduced, with the objective of both increasing DNP efficiency and versatility.[26–54] These range from

[a]*Centre de RMN à Hauts Champs de Lyon, UMR 5082, Université de Lyon (CNRS/ENS Lyon/UCBL), 5 rue de la Doua, Villeurbanne, 69100, France. E-mail: anne.lesage@ens-lyon.fr*

[b]*Center of Magnetic Resonance (CERM), University of Florence, 50019, Sesto Fiorentino, Italy*

[c]*Department of Chemistry 'Ugo Schiff', University of Florence, Via della Lastruccia 13, 50019 Sesto Fiorentino, FI, Italy*

[d]*Consorzio Interuniversitario Risonanze Magnetiche Metalloproteine Paramagnetiche (CIRMMP), Via Luigi Sacconi 6, 50019 Sesto Fiorentino, FI, Italy. E-mail: moreno.lelli@unifi.it*

[e]*Aix Marseille Uni, CNRS, ICR, 13013 Marseille, France. E-mail: olivier.ouari@univ-amu.fr*

[f]*Department of Chemistry and Applied Biosciences, Eidgenössische Technische Hochschule Zürich, CH-8093 Zürich, Switzerland*

[g]*Bruker Biospin, 76275 Ettlingen, Germany*

[h]*Laboratory of Magnetic Resonance, Institut des Sciences et Ingénierie Chimiques, École Polytechnique Fédérale de Lausanne (EPFL), CH-1015 Lausanne, Switzerland*

[i]*National High Magnetic Field Laboratory, Florida State University, Tallahassee, FL 32310, USA*

† Electronic supplementary information (ESI) available: All experimental details such as detailed synthetic procedures, dynamics nuclear polarization NMR spectroscopy, EPR data and MD protocols. See DOI: https://doi.org/10.1039/d4sc04473h

‡ L. N., G. C. and G. M. contributed equally to this work.

hybrid molecular structures coupling a narrow electron paramagnetic resonance (EPR) line radical, such as tetrathiatriarylmethyl-based trityls or BDPA, with a nitroxide,[34,40,42,44,47,51] to metal ion complexes,[41,43,49] mixed-valence compounds,[37,48] or biradicals based on two tethered nitroxides.[26–33,35,36,38,39,45,46,50,52,54] These latter PAs rely on the cross-effect (CE) mechanism to transfer polarization.[55,56] This transfer scheme is effective when the so-called CE matching condition is satisfied, *i.e.* when the difference between the Larmor frequencies of two unpaired electron spins matches the Larmor frequency of the target nucleus,[57–60] which for dinitroxides is achieved as a result of their wide EPR line, that is inhomogeneously broadened by the anisotropy of the *g*-tensors. The efficiency of the CE mechanism depends on the strength of hyperfine coupling between the nucleus and one of the two electrons as well as dipolar and exchange couplings between the two electrons. Under MAS conditions, the magnetic field dependence of CE DNP becomes quite complex due to the interplay between adiabatic crossing events.[58] The efficiency decreases following a trend between $B_0^{-1}$ and $B_0^{-3}$, depending on the specific parameters of the radical.[61] Following the introduction of the first generation of dinitroxides,[26–28] TEKPol[30] and AMUPol[32] were introduced based on key design concepts in the early 2010s. Under standard MAS DNP conditions at 9.4 T and sample temperatures of 100 K they yield more than 200-fold proton NMR signal enhancements ($\varepsilon_H$) in frozen glassy solutions, (and up to a factor 350 with optimized instrumentation[62]). In the following years, attention has been dedicated to further improving the overall sensitivity gain[63–65] in MAS DNP experiments through a detailed understanding of the parameters that drive PA efficiency. In 2016, Kubicki *et al.* compared a collection of more than 30 dinitroxides derived from a variety of molecular scaffolds, including bTurea, PyPol, and bTbk.[35] In another systematic study, Sauvée *et al.* focused on 18 water-soluble bTurea derivatives, functionalized with a range of bulky groups around the N–O moiety or with various substituents on the linker so as to drive design principles.[33] AsymPol radicals featuring a short tether and a conjugated carbon–carbon double bond in a five-membered ring nitroxide, were later introduced.[39] These investigations, backed up with numerical studies[66–70] established that sizeable electron–electron couplings, near-orthogonal *g*-tensors, as well as long electron relaxation times can constructively add up to improve the DNP performance of dinitroxides. Lately, the local geometry around the unpaired electrons has been identified as an additional parameter that governs the efficiency of the DNP process.[45] New AMUPOL-based radicals with an 'open'-ring conformation in the vicinity of the nitroxide groups were proposed, including HydrOPol that yields enhancements as high as 330 at 9.4 T and 100 K. These principles were then shown to transfer to the AsymPol family with the introduction of cAsymPol-POK and cAsymPol-TEK.[50,54] Finally, it was recently shown that strong electron-nuclear hyperfine couplings and a proton-dense environment provide spin-diffusion pathways to rapidly transport hyperpolarization away from the biradical molecule into the bulk of the sample, leading to the development of the high-performance TEKPol derivative NaphPol.[52] Venkatesh *et al.* reported a systematic evaluation of the overall sensitivity gains provided by a series of 18 dinitroxides at 9.4 T, concluding that a glass ceiling in DNP performance for CE dinitroxide biradicals might have been reached at this magnetic field.[71] Most of these studies were carried in a relatively slow MAS regime (typically at 10 kHz) where depolarization losses[58,65,72] are modest and the overall benefit in sensitivity for CE DNP[73] remains high.

Despite this progress, transposing these developments from 9.4 T to the highest fields and fastest MAS frequencies available today is still a bottleneck. The electron-to-nucleus polarization transfer occurs through a series of adiabatic rotation-induced energy level crossings, the efficiency of which is sensitive to the magnetic field and the MAS frequency.[58,65] Thus, as the breadth of the EPR profile of PAs scales with the magnetic field, the saturation of electron spin transitions by the microwave irradiation becomes less effective, and the CE event has a lower probability. In addition, depolarization losses[58,65,72] increase at fast MAS for dinitroxides having medium-sized intramolecular magnetic couplings.[74]

Hybrid biradicals such as TEMtriPols,[34,51] HyTEKs,[40] NATriPols,[44] SNAPols[47] or PyrroTriPol[51] recently appeared as promising PAs for DNP at high magnetic fields (≥18.8 T) and fast MAS. The narrow EPR line of one of the two radical units facilitates the saturation of the corresponding electron. In the case of HyTEK2, this combines with a strong electron–electron hyperfine coupling, giving a DNP efficiency that increases with the magnetic field increase.[40,75] In parallel, efforts have also been devoted to refining the structure of dinitroxides so as to make them efficient at high-field and fast spinning, mostly by tailoring the strength of the intramolecular magnetic couplings. This led to the recently introduced TinyPol[46] families of water-soluble dinitroxides, designed to have a relatively short linker and therefore sizeable electron–electron dipolar and *J*-exchange interactions. However, these radicals provide DNP efficiencies at 18.8 T that are still significantly lower than their analogs at 9.4 T.

Here, capitalizing on key design principles established for dinitroxides at intermediate magnetic fields, we introduce a new series of water-soluble dinitroxide biradicals with scaffolds augmented by dihydroxypropyl antenna chains that perform significantly better than previous dinitroxides at 18.8 T. We find that the new radical M-TinyPol$(OH)_4$ yields enhancement factors of ∼220 at 18.8 T and 60 kHz MAS. The radicals are designed to improve the transfer of polarization away from the molecule and into the bulk, and this is validated by $^2$H ESEEM measurements to probe solvent accessibility supported by Molecular Dynamics simulations and by experiments on deuterated samples. This provides a rational understanding of why the dihydroxypropyl chains present in the best-performing structures are essential to deliver the polarization to the bulk solution.

## Results and discussion

### TinyPol structures

We recently introduced TinyPol and M-TinyPol, for DNP at 18.8 T.[46] The good performance ($\varepsilon_H$ ∼80–90) observed for these

Table 1 Radicals investigated in this work, their DNP performance, and results of EPR measurements. Columns 1 and 2 show the names and the molecular structures respectively, columns 3 and 4 report respectively the proton MAS DNP enhancements and polarization build-up times. All the DNP data were measured in $d_8$-glycerol/$D_2O$/$H_2O$ 60/30/10 (v/v/v) at 18.8 T in 1.3 mm rotors, 105 ± 5 K and 40 kHz MAS, with a radical concentration of 10 mM. The sample temperature was carefully monitored with KBr and equilibrated for the microwave on and off measurements. Columns 6 and 7 show the electron spin relaxation parameters, $T_{ir}$ and $T_m$. The relaxation parameters were measured at W band at 105 K using 100 μM solutions in $d_8$-glycerol/$D_2O$/$H_2O$ 60/30/10 (v/v/v). Column 8 reports the solvent accessibility parameter extracted from EPR ESEEM experiments at 50 K using 200 μM solutions in $d_8$-glycerol/$D_2O$/$H_2O$ 60/30/10 (v/v/v) as detailed in the ESI.† Column 9 shows the weighted average of the exchange coupling |$J$|, measured with room-temperature X-band EPR from a fitting procedure using EasySpin[76] as detailed in the ESI†

| | | DNP performance, 18.8 T, 40 kHz MAS | | | | EPR parameters | | | |
|---|---|---|---|---|---|---|---|---|---|
| Radical | Structure | $\varepsilon_H$ | $T_{B,ON}$ (s) | $\varepsilon_H/\sqrt{T_{B,ON}}$ | $\varepsilon_{DEPO}$ | $T_{ir}$ (μs) | $T_m$ (μs) | $\Pi(D_2O)$ | $\langle\lvert J\rvert\rangle$ (MHz) |
| TinyPol-NH | 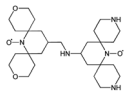 | 71 ± 4 | 25.4 ± 1 | 14.1 | n.d. | 306 ± 14 | 6.8 ± 0.4 | 0.37 ± 0.04 | 14.1 |
| O-TinyPol | 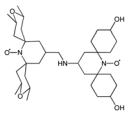 | 110 ± 5 | 9.3 ± 0.5 | 36.1 | n.d. | 284 ± 14 | 3.3 ± 0.4 | 0.37 ± 0.04 | 27.7 |
| TinyPol(OH)$_4$ | 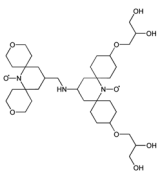 | 130 ± 6 | 8.9 ± 0.5 | 43.0 | n.d. | 250 ± 13 | 6.9 ± 0.4 | 0.34 ± 0.03 | 29.2 |
| O-TinyPol(OH)$_4$ | 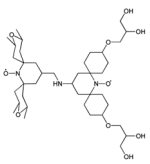 | 159 ± 6 | 8.3 ± 0.5 | 55.0 | 0.68 | 258 ± 13 | 2.8 ± 0.1 | 0.35 ± 0.03 | 27.1 |
| M-TinyPol | 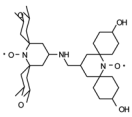 | 124 ± 6 | 16.8 ± 1 | 30.2 | 0.86 | 256 ± 14 | 1.9 ± 0.2 | 0.3 ± 0.04 | 25.3 |
| M-TinyPol(OH)$_4$, (M-TinyPol(OH)$_4$)-$d_{10}$) | 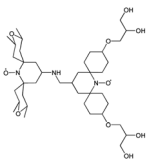 | 138 ± 7, (103 ± 5) | 7.5 ± 0.5, (8.6 ± 0.4) | 50.4, (35.1) | 0.68 | 251 ± 13 | 2.9 ± 0.1 | 0.32 ± 0.03 | 27.5 |
| AsymPol-POK | 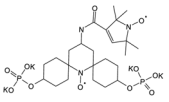 | 75 ± 7 | 4.4 ± 0.2 | 37.6 | 0.66 | 199 ± 10 | <2.00 | 0.43 ± 0.04 | 80.5[a] |

[a] This value is from ref. 39.

radicals was accounted for by an increase in the magnetic interactions between the two unpaired electrons. In this work, five new tailored TinyPol structures were prepared following updated design principles. Their structures, as well that of M-TinyPol[46] and AsymPol-POK,[39] are shown in Table 1. Details regarding the synthesis of the molecules are provided in the ESI.† The structure of TinyPol is presented in the ESI (Scheme 1†) as a reminder.

TinyPol-NH, O-TinyPol, TinyPol(OH)$_4$ and O-TinyPol(OH)$_4$ are based on the TinyPol scaffold while M-TinyPol(OH)$_4$ is derived from M-TinyPol. The functionalization of the spirocyclohexyl rings with aliphatic chains bearing hydroxyl groups increases the molecular weight of TinyPol(OH)$_4$, O-TinyPol(OH)$_4$ and M-TinyPol(OH)$_4$ structures as well as the hydrogen bonding interactions with the frozen matrix. This is first expected to lengthen the electron spin relaxation times,

which is beneficial for their DNP performance. This design principle is well established since the development of bCTbK[31] and TEKPol[30] derivatives and is now embedded in most contemporary dinitroxide PAs.[50,52,54,71] The local density of protons around the unpaired electron was also suggested to be a key parameter that modulates the DNP performance of dinitroxides at 9.4 T. Using a series of deuterated compounds, Venkatesh *et al.* recently demonstrated that the PA protons located beyond the cyclohexyl groups in TEKPoL play a key role in the DNP process,[52] relaying the hyperpolarization outside of the spin diffusion barrier,[77] as postulated by Perras *et al.* from simulations.[78] Here, the chains decorating the cyclohexyl rings are potentially expected to play a similar role.

The local structure around the nitroxide, with open (O-) or closed (C-) conformations for the tetrahydropyran groups was also shown to significantly affect the efficiency of the DNP process in AMUPol, PyPol and PyTol derivatives,[45] and this was tentatively correlated to the accessibility of solvent molecules to unpaired electrons. Fully open conformers were shown to outperform nitroxides with closed conformations. Locking the conformation of the tetrahydropyran rings in the O-form was achieved by introducing stereo-controlled *cis*-2,6 dimethyl groups.

This effect was then exploited in cAsymPolTEK where the "open" forms were again found to be significantly more efficient.[54] Here, M-TinyPol and M-TinyPol(OH)$_4$ have fully open conformations on one side of the molecule, as is the case for O-TinyPol(OH)$_4$ which is the open (O-) conformer of TinyPol(OH)$_4$.

In unsubstituted tetrahydropyran rings, various conformations including the O- and C- conformations co-exist. This is the case for the left side of TinyPol-NH and TinyPol(OH)$_4$ molecules in Table 1. The functionalization of the cyclohexanol rings with the dihydroxylpropyl chains has no impact on the stereochemical constraints, and thus half-open and half-closed conformations are maintained.

We find such conformations in TinyPol(OH)$_4$, O-TinyPol(OH)$_4$, M-TinyPol and M-TinyPol(OH)$_4$ in the right side of the structures according to schemes of Table 1. The DFT optimized structures of the six structures in the series are reported in Fig. S16.†

Molecular dynamics (MD) simulations were carried out to probe the conformational space of the PAs investigated here. Fig. 1(a) and (b) report respectively the distribution of angles between the two nitroxide planes and electron–electron distances. All TinyPols show one main e–e distance, between 10.4 and 10.8 Å, corresponding to an e–e dipolar coupling of ~45 MHz. These dipolar couplings $D$, together with the exchange $J$-couplings drive the DNP cross-effect mechanism. MD trajectories highlight two main angles with broad distributions, at around 20° and 110–130° for O-TinyPol, TinyPol(OH)$_4$ and O-TinyPol(OH)$_4$, and three angles at around 50–60°, 80–100° and 120–160° for TinyPol-NH, M-TinyPol and M-TinyPol(OH)$_4$. Individual plots are displayed in Fig. S17 and S18† for 5 MD runs.

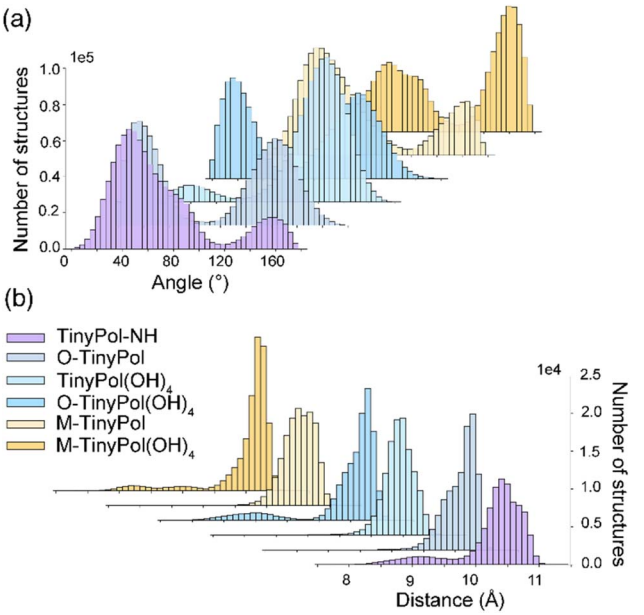


Fig. 1 (a) and (b) Angle and distance distribution between the two unpaired electrons obtained from MD simulations. The distance was calculated by setting the position of the electron at the middle of the NO bond. The angle is between the two nitroxide planes. For each TinyPol structure, the results of 5 MD runs are reported separately in the ESI (Fig. S17 and S18†).

## Electron relaxation properties

Fig. 2 reports the measured electron relaxation times. The $T_{ir}$ were found to be quite similar across the series, ranging between 250 and 306 μs, while the $T_m$ vary between around 2 and 7 μs. The latter are shortened in biradicals presenting an open conformation on one side of the molecule, most likely due to the presence of the methyl groups.[30] Due to the disparity in $T_m$, the saturation factors (defined as the product of $T_{ir}$ and $T_m$) in turn range across an order of magnitude, from *ca.* 220 μs$^2$ for M-TinyPol to *ca.* 2080 μs$^2$ for TinyPol-NH as displayed in Fig. S15.†

Electron relaxation times were also measured for AsymPol-POK.[39] Values significantly shorter than those of TinyPols were obtained as reported in Table 1, in line with expectations.[31]

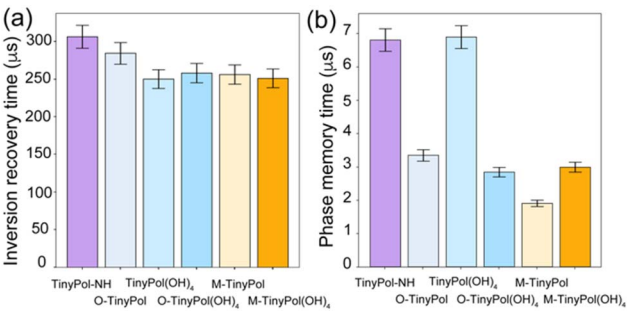


Fig. 2 (a) Electron inversion recovery time ($T_{ir}$) and (b) electron phase memory time ($T_m$), for the six radicals investigated here. The electron relaxation parameters were measured at W band at 105 K using 100 μM solutions in $d_8$-glycerol/$D_2O$/$H_2O$ 60/30/10 (v/v/v).

### DNP performance

The DNP performance (enhancement $\varepsilon_H$ and build-up times $T_{B,ON}$) at 18.8 T and 40 kHz MAS of the TinyPol derivatives investigated here is summarized in Table 1 for 10 mM radical in $d_8$-glycerol/$D_2O$/$H_2O$ 60/30/10 (v/v/v). As a reference, experimental data are also reported for AsymPol-POK.

We also report in Table 1 the sensitivity factor $\varepsilon_H/\sqrt{T_{B,ON}}$, which is a more relevant reporter of the overall DNP efficiency than $\varepsilon_H$ alone,[63,65,73] as short polarization build-up times can compensate for lower enhancements, and *vice versa*. Depolarization values are reported in Table S7† for some of the structures. We first observe that TinyPol-NH yields a relatively modest enhancement of ~70, despite its large saturation factor as well as long polarization build-up time (>25 s). O-TinyPol, which is the open form of TinyPol, yields to a sizeable 110-fold enhancement factor. A further increase of $\varepsilon_H$ is observed upon addition of dihydroxypropyl chains to the spirocyclohexyl groups, on one side of the radical, in place of the NH or OH groups for TinyPol(OH)$_4$ and its open version O-TinyPol(OH)$_4$. The build-up times for these three polarizing agents are significantly shorter than those of TinyPol-NH, reflecting a much faster polarization transfer rate to the bulk solution.[77] In particular O-TinyPol(OH)$_4$ has a relatively short DNP build-up time, which combined with $\varepsilon_H$ ~160 maximizes $\varepsilon_H/\sqrt{T_{B,ON}}$. Similarly, the addition of the dihydroxypropyl chains to the M-TinyPol scaffold leads to a higher enhancement factor. Thus, M-TinyPol(OH)$_4$ reaches almost 140-fold enhancement factors at 40 kHz MAS. M-TinyPol(OH)$_4$ also displays a significantly shorter $T_{B,ON}$ than M-TinyPol. Both effects combine to yield a high $\varepsilon_H/\sqrt{T_{B,ON}}$ value.

In Fig. 3, overall sensitivity gains are calculated for O- and M-TinyPol(OH)$_4$, and compared with the values measured for the reference M-TinyPol and AsymPol-POK radicals under similar experimental conditions. They were calculated from the proton enhancement $\varepsilon_H$, scaled by the depolarization factor, and considering the gain of a shorter build-up time $T_{B,ON}$ with respect to the pure solvent $T_1$ (see ESI† for the detailed calculation of $\Sigma'$). M-TinyPol(OH)$_4$ yields a gain of *ca.* 75% at 10 kHz MAS and 40% at 40 kHz MAS with respect to M-TinyPol. O-TinyPol(OH)$_4$ also yields excellent performance at fast spinning frequencies.

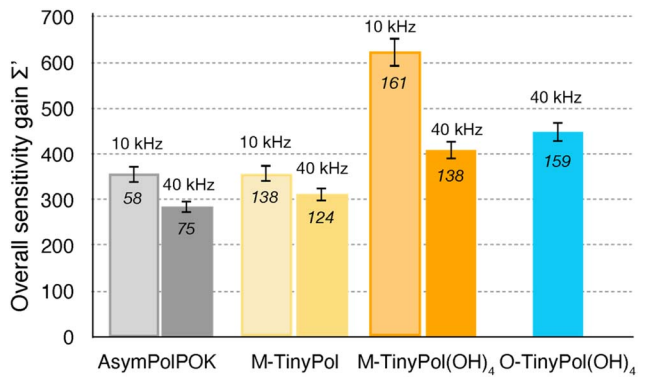


Fig. 3 Overall sensitivity factors of 10 mM M-TinyPol, AsymPol-POK, M-TinyPol(OH)$_4$ and O-TinyPol(OH)$_4$ solutions in $d_8$-glycerol/$D_2O$/$H_2O$ 60/30/10 (v/v/v) acquired at 18.8 T in 1.3 mm zirconia rotors at 10 or 40 kHz MAS frequencies. The sample temperature was ~110 K. The overall sensitivity factor is calculated as the product of $\varepsilon_H$, the depolarization factor, and the square root of the ratio between the pure solvent $T_1$ and the polarization build-up time $T_{B,ON}$, as described in the ESI.† Notably, in this calculation, the paramagnetic quenching factor was not considered, while signal losses due to depolarization, as well as the value of $T_{B,ON}$, were taken into account. Enhancement factors $\varepsilon_H$ are indicated in italic.

While the superior performance of M-TinyPol(OH)$_4$ over M-TinyPol could be tentatively ascribed to a higher saturation factor (or in other words to a better saturation of the electron spin transition due to a significantly longer $T_m$, as shown in Fig. 2), such an argument does not explain the higher DNP efficiency of O-TinyPol(OH)$_4$ with respect to TinyPol(OH)$_4$. This suggests that the DNP performance of these dinitroxides is not only governed by their electron spin relaxation behavior, and that other parameters must be considered.

The relative orientation of the electron *g*-tensors could be one of these factors. Due to the flexibility of the linker, all TinyPol radicals investigated here display 2 to 3 main conformations, with distributions in the relative orientations of the nitroxide planes as reported by the MD simulations (Fig. 1(a)). Notably, only a small fraction of those distributions displays an optimal orientation with the two *g*-tensors in orthogonal planes.[28,66,79] However, no correlation could be established between the distribution of conformations probed by MD at ambient temperature and the DNP performance. In contrast, we observe that M- and O-TinyPol(OH)$_4$ have different distribution of *g*-tensor orientations but similar sensitivity factors $\varepsilon_H/\sqrt{T_{B,ON}}$. Thus, while at cryogenic temperatures the distributions of conformations might be different, disparities in the relative orientation of the *g*-tensors does not appear to explain the differences observed in DNP performance within the TinyPol series.

The $\varepsilon_H$ and $T_{B,ON}$ values reported in Table 1 were measured in non-degassed solutions. However, paramagnetic oxygen ($O_2$) dissolved within the DNP matrix, even at low concentration, is expected to act as effective relaxation sinks that will decrease the $^1$H polarization build-up time constant and in turn lead to a less efficient propagation of the hyperpolarization from the dinitroxides. Griffin and co-workers have recently showed that solid-effect enhancement of the water-soluble $NMe_3$-BDPA radical in DNP juice, where build-up times were on the order of 60 s, could be improved by almost a factor 2 by degassing the sample.[80] To evaluate if this effect is still observable for shorter build-up times, measurements were carried out for 10 mM O-TinyPol(OH)$_4$ in both degassed and non-degassed solutions. The results (Fig. S21†) show only a moderated increase in the enhancement factors and polarization build-up times, leading to an increase in overall sensitivity of between 5 and 15%.

### Local proton density around the unpaired electron

To better understand the origin of the observed improved performances, we first turn our attention to the solvation of nitroxide moieties in the DNP matrix. The solvent accessibility

was tentatively suggested to be a key parameter that modulates the density of protons around the unpaired electrons and in turn the DNP performance of dinitroxides at 9.4 T.[45] This was based on the observation of a difference in solvent accessibility between fully open and fully closed conformations of the same radicals. To assess this effect, three pulse ESEEM experiments were conducted to probe proximities between the unpaired electron and the deuterated molecules in the matrix. The calculated solvent modulation depth $k_D$ and solvent accessibility parameter $\Pi$ (solvent) can be interpreted as an estimation of the number of deuterons present on a length scale in the range of 3 to 6 Å from the unpaired electrons, as the contribution of directly bonded nuclear spins is suppressed.[81] All data are reported in Table S3† (and Fig. S11†), as well as details of the calculations of the $k_D$ and $\Pi$ parameters. Table 1 shows the extracted solvent accessibility $\Pi$ parameters. All the TinyPol-like radicals here have similar accessibility to solvent molecules. This result is not surprising, considering the similar polarity around the unpaired electron and the available space nearby (the open or free conformations of the tetrahydropyran rings do not significantly reduce the access of solvent molecules, see DFT optimized structures of Fig. S16†).

In the light of recent work done by Griffin and co-workers,[82] Bennati and co-workers[83] as well as Stoll and co-workers,[84] ESEEM experiments were conducted on solutions of M-TinyPol and TinyPol(OH)$_4$, in either $h_8$-glycerol/$D_2O$ 60/40 (v/v) or $d_5$-glycerol/$H_2O$ 60/40 (v/v). Both of these solutions have *ca.* 40% $^2$H content, but with a different distribution, as almost all the deuterium atoms are on the water molecules in the first case while sitting on the non-exchangeable positions of glycerol in the second case. The results of these experiments are summarized in Fig. 4(a) and Table S4.†

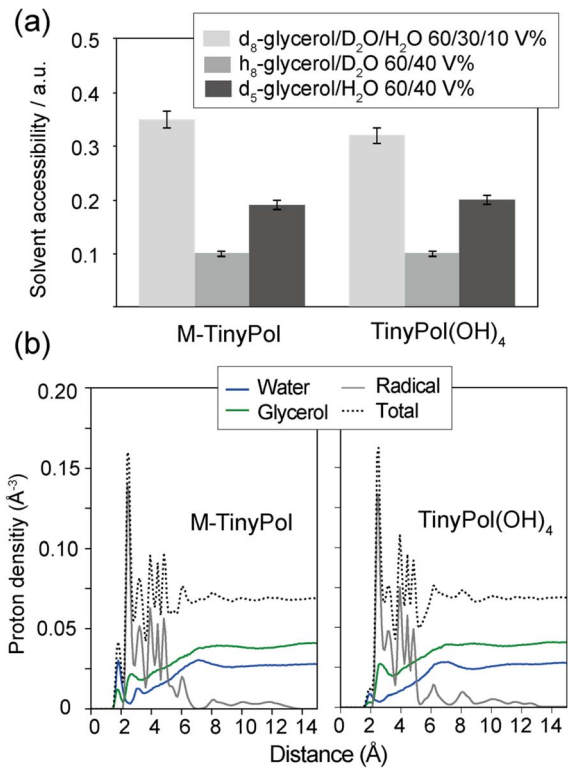


Fig. 4 (a) Solvent accessibility parameters measured by X-band ESEEM experiments in 200 μM solutions of M-TinyPol and M-TinyPol(OH)$_4$ in differently deuterated glycerol/water mixtures at 50 K. (b) Radial proton density distribution in a spherical range of 0 to 15 Å from the oxygen atom of the nitroxide group, calculated from MD simulations run in a glycerol/water 60/40 (v/v) mixture at 293 K as detailed in the ESI:† water protons (blue), glycerol protons (green), protons belonging to the biradical itself (grey).

We observed that the modulation depth and accessibility parameter are similar for M-TinyPol and TinyPol(OH)$_4$ for all the three deuterated matrices tested, *i.e.* are independent on the biradical structure. However, both biradicals yield significantly different accessibility parameters using solvent mixtures with different deuterium distribution. More specifically, the $^2$H accessibility value almost doubles in $d_5$-glycerol/$H_2O$ 60/40 compared to $h_8$-glycerol/$D_2O$ 60/40 (v/v) (Fig. 4(a)). The enhanced modulation of the echo decay of the electrons, driven by distance-dependent hyperfine couplings, in $d_5$-glycerol/$H_2O$ 60/40 (v/v) implies that there are more deuterons at a distance of 3 to 6 Å from the unpaired electrons in this solvent mixture. Similar observations were made for O-TinyPol(OH)$_4$ (Fig. S12†). As deuterons are located only on glycerol (at non-exchangeable sites), this result points towards the predominance of glycerol deuterons at this 3 to 6 Å range, which matches roughly the size of the spin diffusion barrier.[77,82,85,86] As expected, the solvent accessibility parameter is even higher when the $d_8$-glycerol/$D_2O$/$H_2O$ 60/30/10 (v/v/v) composition, the so-called "DNP juice", is used, where glycerol molecules are fully deuterated, although susceptible to exchange with the 10% protonated water molecules. Overall, these data suggest that the shell volume surrounding the unpaired electrons, between 3 and 6 Å, is mostly occupied by deuterons from glycerol molecules, and this distribution is substantially similar for all TinyPol-like radicals.

To further interpret these results, the radial proton density in a sphere of 15 Å from the oxygen atom of the nitroxide group was calculated from 8001 snapshots from MD trajectories carried out in a glycerol/water 60/40 (v/v) mixture at 293 K. Calculations were done on both sides of the PA and average values were computed (as detailed in the ESI†). Fig. 4(b) shows the result of these calculations for M-TinyPol and TinyPol(OH)$_4$. The plots for the other TinyPols in the series are presented in Fig. S20.† In both cases, these calculations indicate that, while the first solvation shell around the NO bond is mostly occupied by hydrogen-bonded water molecules with protons at about 2 Å distance from the oxygen atom, glycerol protons are predominant beyond this distance. Notably the glycerol molecules around the nitroxide yield a significant $^1$H density from 3 to 6 Å. This corroborates the ESEEM data.

Other recent investigations pointed out the key role of protons in the vicinity of the unpaired electrons, not only to allow an efficient CE DNP transfer through strong hyperfine couplings, but also to carry the hyperpolarization across the spin diffusion barrier away from the PA.

Notably, it was postulated[78] and then demonstrated in TEKPoL that phenyl protons located in a 6 to 9.5 Å range from the unpaired electrons, are essential to transport the polarization into the bulk.[52] Here, the ESEEM EPR data and the MD

simulations show that deuterons from glycerol molecules, which unlike protons, cannot convey the $^1$H hyperpolarization across the spin diffusion barrier, are predominant in the second solvation shell of the nitroxide at a 2 to 4 Å range distance from the unpaired electron. Their presence may partly hinder the propagation of the hyperpolarization. In this regard, we hypothesize here that the hydroxypropyl chains in TinyPol(OH)$_4$, O-TinyPol(OH)$_4$ and M-TinyPol(OH)$_4$ create pathways to relay the polarization to the bulk sample by proton spin-diffusion, in analogy to the aromatic antenna groups in NaphPol.[52] Note that it was recently shown by simulations that in AsymPol series, radical protons in the vicinity of the unpaired electrons may not be necessary to relay the polarization.[87]

To validate this hypothesis, a deuterated version of M-TinyPol(OH)$_4$ was prepared, in which the protons of the hydroxypropyl chains were replaced by deuterons. Fig. 5 compares the enhancement and build-up times in protonated and deuterated M-TinyPol(OH)$_4$ as a function of the spinning frequency. Deuteration of the side chains leads to lower enhancement factors and longer build-up times. This observation is in line with what was observed for a series of deuterated TEKPoL PAs, where $^1$H DNP enhancements were shown to decrease with higher biradical deuteration levels while the DNP build-up times concomitantly increased, almost all the deuterated forms having lower $\varepsilon_H$ and longer $T_{B,ON}$ than the protonated radical.[52] This also confirms that the protons in the chains provide new channels to propagate the hyperpolarization to the bulk, resulting in superior overall DNP performance, *i.e.* shorter polarization build-up time or higher polarization transfer coefficient at the spin diffusion barrier interface $k_{DNP}$, according to the model of Prisco and co-workers.[77]

We note that the $\varepsilon_H/\sqrt{T_{B,ON}}$ factor drops from 50 to 35 upon deuteration, *i.e.* the overall sensitivity of deuterated M-TinyPol(OH)$_4$ almost returns to that of M-TinyPol (Table 1), which differs from M-TinyPol(OH)$_4$ only by the absence of the hydroxypropyl chains.

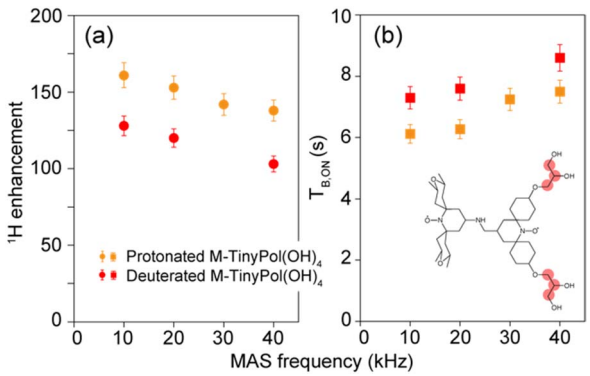


Fig. 5 (a) Enhancement factors and (b) polarization build-up times of protonated and deuterated M-TinyPol(OH)$_4$ at a 10 mM concentration in bulk solutions of $d_8$-glycerol/$D_2O$/$H_2O$ 60/30/10 (v/v/v), as a function of MAS frequency. Enhancements values were measured at 18.8 T from proton NMR spectra in 1.3 mm zirconia rotors at a sample temperature of 110 ± 5 K. Experimental details are given in the ESI.† The position of the deuterons are indicated by pale red circles in the molecular structure of M-TinyPol(OH)$_4$.

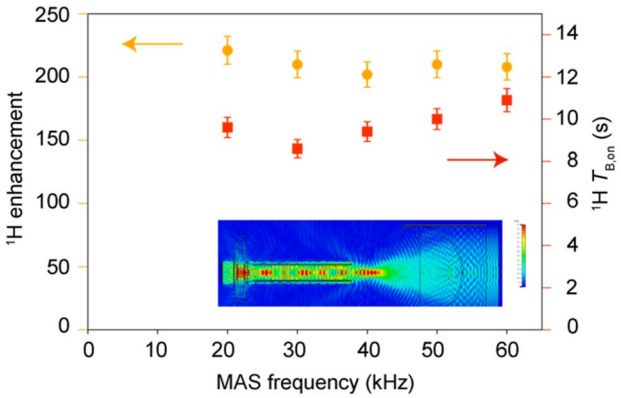


Fig. 6 Enhancement factors and polarization build-up times of 10 mM M-TinyPol(OH)$_4$ in a bulk solution of $d_8$-glycerol/$D_2O$/$H_2O$ 60/30/10 (v/v/v), as a function of MAS frequency. Enhancements values were measured at 18.8 T from proton NMR spectra, in a 0.7 mm zirconia rotor at a sample temperature of 110 ± 5 K. The inset shows the microwave distribution within the rotor predicted by finite-element simulations.

### Performance of M-TinyPol(OH)$_4$ at very fast MAS

The performance of M-TinyPol(OH)$_4$ at MAS rates up to 60 kHz measured in a 0.7 mm DNP probe is shown in Fig. 6. The predicted μ-wave distribution within the rotor was calculated from finite-element simulations and is displayed as an inset in Fig. 6. The average microwave field is calculated to be slightly higher than in 1.3 mm rotors 1.76 *versus* 1.07 MHz//W$^{-1/2}$). Here, we note that there are several reasons for the superior μ-wave performance of the 0.7 mm probe. First, the portion of the sample volume that is irradiated by the beam is about 10% larger compared to that of a 1.3 mm rotor (Fig. S23†). Furthermore, the beam transmitted through the probe's waveguide is focused to a smaller diameter thereby increasing the intensity of the microwave $B_1$ field. While the thicker zirconia wall of the 1.3 mm rotor also introduces more losses, its impact on the $B_1$ field strongly depends on the wall thickness-to-wavelength ratio due constructive *versus* destructive interference, as detailed in the ESI.† Enhancement factors of between 204 and 214 were measured over the whole spinning frequency range, with build-up times ranging from 8.5 to 11 s. These values are the highest reported so far for dinitroxides at high fields and fast MAS frequencies, highlighting the importance of the instrumentation and of efficient microwave penetration to obtain high signal amplification.[88,89]

## Conclusion

In summary, a series of new TinyPol radicals were synthesized and their DNP performance was examined at 18.8 T, 100 K and 40 kHz MAS. We find that the introduction of protonated hydroxypropyl chains decorating the spirocyclohexyl groups around the nitroxide rings significantly improves the DNP efficiency of TinyPol radicals, both in terms of enhancement factors, $^1$H DNP build-up times and overall sensitivity gain. Combining this novel structural element with a nitroxide

having an open conformation of the tetrahydropyran rings results in O-TinyPol(OH)$_4$ and M-TinyPol(OH)$_4$ that provide a sensitivity gain almost twice that of previously reported dinitroxides.

We find that deuteration of the hydroxypropyl chains decreases enhancement factors while increasing build-up times, suggesting that protons located in the chains (*i.e.* close to but not in the immediate vicinity of the electrons) are key to transporting polarization across the spin diffusion barrier into the bulk.[52,77] This analysis is supported with $^2$H ESEEM measurements and MD simulations that suggest that the deuterated glycerol molecules of the DNP matrix are located mainly in the second solvation shell of the NO bond, limiting access to protonated water molecules. Overall, this provides a rational framework for why protons in the chains are important to delivering the polarization to the bulk solution, and provides a clear guideline for the future developments of new polarizing agents but also of optimized formulations.

## Data availability

Data that support the findings of this study are available from the corresponding author upon reasonable request. The data supporting this article have been included as part of the ESI.†

## Author contributions

L. N., G. M., S.-E. A., D. G., A. V., Z. W., T. R. conducted and analysed DNP NMR experiments. L. N. developed and conducted the molecular dynamic simulations. L. N and D. S. ran the DFT calculations. M. Y., L. N. and G. M. conducted EPR measurements. G. C. and O. O. synthesised the radicals. C. R. and A. P. did the finite-element simulations. A. L., M. L. and O. O. conceptualized the research in close consultation with L. E. and acquired necessary funding. All authors participated in the analysis and discussion of the experiments, and related results. The manuscript was written through contributions of all authors. All authors have given approval to the final version of the manuscript.

## Conflicts of interest

There are no conflicts to declare.

## Acknowledgements

We gratefully acknowledge Laura Troussicot, Gunnar Jeschke, and Judith Schlagnitweit for constructive advice and discussion on this work. This work was supported by Swiss National Science Foundation Grant No. 200020_212046, EU H2020-INFRAIA Grant No. 101008500, the ANR contract ANR-22-CE09-0017-01 and H2020 Marie Skłodowska-Curie Individual fellowship (grant number 101024369). ML and LN thank Fondazione Cassa di Risparmio di Firenze for funding. The financial support provided by the MUR – Dipartimenti di Eccellenza 2023–2027 (DICUS 2.0) to the Department of Chemistry "Ugo Schiff" of the University of Florence is acknowledged. ML and LN acknowledge the contribution of the "Università Italo-Francese/Université Franco-Italienne (UIF/UFI), project number: C2-224. We gratefully acknowledge financial support from IR INFRANALYTICS FR2054 for enabling this research. LN gratefully acknowledges support from the PSMN (Pôle Scientifique de Modélisation Numérique) of the ENS de Lyon for the computing resources. C. Thieuleux, C. Camp and L. Veyre (CP2M laboratory in Lyon) are acknowledged for their help with the Schlenk and glovebox techniques.

## Notes and references

1 B. Reif, S. E. Ashbrook, L. Emsley and M. Hong, Solid-state NMR spectroscopy, *Nat. Rev. Methods Primers*, 2021, **1**, 2.
2 Q. Z. Ni, E. Daviso, T. V. Can, E. Markhasin, S. K. Jawla, T. M. Swager, R. J. Temkin, J. Herzfeld and R. G. Griffin, High Frequency Dynamic Nuclear Polarization, *Acc. Chem. Res.*, 2013, **46**, 1933–1941.
3 A. J. Rossini, A. Zagdoun, M. Lelli, A. Lesage, C. Copéret and L. Emsley, Dynamic Nuclear Polarization Surface Enhanced NMR Spectroscopy, *Acc. Chem. Res.*, 2013, **46**, 1942–1951.
4 R. G. Griffin, T. M. Swager and R. J. Temkin, High frequency dynamic nuclear polarization: New directions for the 21st century, *J. Magn. Reson.*, 2019, **306**, 128–133.
5 B. Corzilius, High-Field Dynamic Nuclear Polarization, *Annu. Rev. Phys. Chem.*, 2020, **71**, 143–170.
6 J. Eills, D. Budker, S. Cavagnero, E. Y. Chekmenev, S. J. Elliott, S. Jannin, A. Lesage, J. Matysik, T. Meersmann, T. Prisner, J. A. Reimer, H. M. Yang and I. V. Koptyug, Spin Hyperpolarization in Modern Magnetic Resonance, *Chem. Rev.*, 2023, **123**, 1417–1551.
7 M. Lelli, D. Gajan, A. Lesage, M. A. Caporini, V. Vitzthum, P. Miéville, F. Héroguel, F. Rascón, A. Roussey, C. Thieuleux, M. Boualleg, L. Veyre, G. Bodenhausen, C. Copéret and L. Emsley, Fast Characterization of Functionalized Silica Materials by Silicon-29 Surface-Enhanced NMR Spectroscopy Using Dynamic Nuclear Polarization, *J. Am. Chem. Soc.*, 2011, **133**, 2104–2107.
8 A. J. Rossini, A. Zagdoun, F. Hegner, M. Schwarzwalder, D. Gajan, C. Coperet, A. Lesage and L. Emsley, Dynamic Nuclear Polarization NMR Spectroscopy of Microcrystalline Solids, *J. Am. Chem. Soc.*, 2012, **134**, 16899–16908.
9 M. Renault, S. Pawsey, M. P. Bos, E. J. Koers, D. Nand, R. Tommassen-van Boxtel, M. Rosay, J. Tommassen, W. E. Maas and M. Baldus, Solid-State NMR Spectroscopy on Cellular Preparations Enhanced by Dynamic Nuclear Polarization, *Angew. Chem., Int. Ed.*, 2012, **51**, 2998–3001.
10 T. Wang, Y. B. Park, M. A. Caporini, M. Rosay, L. H. Zhong, D. J. Cosgrove and M. Hong, Sensitivity-enhanced solid-state NMR detection of expansin's target in plant cell walls, *Proc. Natl. Acad. Sci. U.S.A.*, 2013, **110**, 16444–16449.
11 H. Takahashi, I. Ayala, M. Bardet, G. De Paëpe, J. P. Simorre and S. Hediger, Solid-State NMR on Bacterial Cells: Selective Cell Wall Signal Enhancement and Resolution Improvement using Dynamic Nuclear Polarization, *J. Am. Chem. Soc.*, 2013, **135**, 5105–5110.

12 L. Protesescu, A. J. Rossini, D. Kriegner, M. Valla, A. de Kergommeaux, M. Walter, K. V. Kravchyk, M. Nachtegaal, J. Stangl, B. Malaman, P. Reiss, A. Lesage, L. Emsley, C. Copéret and M. V. Kovalenko, Unraveling the Core–Shell Structure of Ligand-Capped Sn/$SnO_x$ Nanoparticles by Surface-Enhanced Nuclear Magnetic Resonance, Mossbauer, and X-ray Absorption Spectroscopies, *ACS Nano*, 2014, **8**, 2639–2648.

13 F. A. Perras, T. Kobayashi and M. Pruski, Natural Abundance $^{17}$O DNP Two-Dimensional and Surface-Enhanced NMR Spectroscopy, *J. Am. Chem. Soc.*, 2015, **137**, 8336–8339.

14 F. A. Perras, T. Kobayashi and M. Pruski, Growing Signals from the Noise: Challenging Nuclei in Materials DNP, *Emagres*, 2018, **7**, 35–50.

15 P. Berruyer, L. Emsley and A. Lesage, DNP in Materials Science: Touching the Surface, *Emagres*, 2018, **7**, 93–104.

16 L. Zhao, A. C. Pinon, L. Emsley and A. J. Rossini, DNP-enhanced solid-state NMR spectroscopy of active pharmaceutical ingredients, *Magn. Reson. Chem.*, 2018, **56**, 583–609.

17 A. G. M. Rankin, J. Trébosc, F. Pourpoint, J. P. Amoureux and O. Lafon, Recent developments in MAS DNP-NMR of materials, *Solid State Nucl. Magn. Reson.*, 2019, **101**, 116–143.

18 K. Jaudzems, T. Polenova, G. Pintacuda, H. Oschkinat and A. Lesage, DNP NMR of biomolecular assemblies, *J. Struct. Biol.*, 2019, **206**, 90–98.

19 T. Wolf, S. Kumar, H. Singh, T. Chakrabarty, F. Aussenac, A. I. Frenkel, D. T. Major and M. Leskes, Endogenous Dynamic Nuclear Polarization for Natural Abundance $^{17}$O and Lithium NMR in the Bulk of Inorganic Solids, *J. Am. Chem. Soc.*, 2019, **141**, 451–462.

20 M. A. Hope, B. L. D. Rinkel, A. B. Gunnarsdóttir, K. Märker, S. Menkin, S. Paul, I. V. Sergeyev and C. P. Grey, Selective NMR observation of the SEI-metal interface by dynamic nuclear polarisation from lithium metal, *Nat. Commun.*, 2020, **11**, 2224.

21 M. Juramy, R. Chèvre, P. C. Vioglio, F. Ziarelli, E. Besson, S. Gastaldi, S. Viel, P. Thureau, K. D. M. Harris and G. Mollica, Monitoring Crystallization Processes in Confined Porous Materials by Dynamic Nuclear Polarization Solid-State Nuclear Magnetic Resonance, *J. Am. Chem. Soc.*, 2021, **143**, 6095–6103.

22 S. Haber and M. Leskes, Dynamic Nuclear Polarization in battery materials, *Solid State Nucl. Magn. Reson.*, 2022, **117**, 101763.

23 T. Biedenbander, V. Aladin, S. Saeidpour and B. Corzilius, Y Dynamic Nuclear Polarization for Sensitivity Enhancement in Biomolecular Solid-State NMR, *Chem. Rev.*, 2022, **122**, 9738–9794.

24 W. Y. Chow, G. De Paëpe and S. Hediger, Biomolecular and Biological Applications of Solid-State NMR with Dynamic Nuclear Polarization Enhancement, *Chem. Rev.*, 2022, **122**, 9795–9847.

25 L. Bhai, J. K. Thomas, D. W. Conroy, Y. Xu, H. M. Al-Hashimi and C. P. Jaroniec, Hydrogen bonding in duplex DNA probed by DNP enhanced solid-state NMR N-H bond length measurements, *Front. Mol. Biosci.*, 2023, **10**, 1286172.

26 K.-N. Hu, H.-h. Yu, T. M. Swager and R. G. Griffin, Dynamic Nuclear Polarization with Biradicals, *J. Am. Chem. Soc.*, 2004, **126**, 10844–10845.

27 C. Song, K.-N. Hu, C.-G. Joo, T. M. Swager and R. G. Griffin, TOTAPOL: A Biradical Polarizing Agent for Dynamic Nuclear Polarization Experiments in Aqueous Media, *J. Am. Chem. Soc.*, 2006, **128**, 11385–11390.

28 Y. Matsuki, T. Maly, O. Ouari, H. Karoui, F. Le Moigne, E. Rizzato, S. Lyubenova, J. Herzfeld, T. Prisner, P. Tordo and R. G. Griffin, Dynamic Nuclear Polarization with a Rigid Biradical, *Angew. Chem., Int. Ed.*, 2009, **48**, 4996–5000.

29 C. Ysacco, H. Karoui, G. Casano, F. Le Moigne, S. Combes, A. Rockenbauer, M. Rosay, W. Maas, O. Ouari and P. Tordo, Dinitroxides for Solid State Dynamic Nuclear Polarization, *Appl. Magn. Reson.*, 2012, **43**, 251–261.

30 A. Zagdoun, G. Casano, O. Ouari, M. Schwarzwälder, A. J. Rossini, F. Aussenac, M. Yulikov, G. Jeschke, C. Copéret, A. Lesage, P. Tordo and L. Emsley, Large Molecular Weight Nitroxide Biradicals Providing Efficient Dynamic Nuclear Polarization at Temperatures up to 200 K, *J. Am. Chem. Soc.*, 2013, **135**, 12790–12797.

31 A. Zagdoun, G. Casano, O. Ouari, G. Lapadula, A. J. Rossini, M. Lelli, M. Baffert, D. Gajan, L. Veyre, W. E. Maas, M. Rosay, R. T. Weber, C. Thieuleux, C. Coperet, A. Lesage, P. Tordo and L. Emsley, A Slowly Relaxing Rigid Biradical for Efficient Dynamic Nuclear Polarization Surface-Enhanced NMR Spectroscopy: Expeditious Characterization of Functional Group Manipulation in Hybrid Materials, *J. Am. Chem. Soc.*, 2012, **134**, 2284–2291.

32 C. Sauvée, M. Rosay, G. Casano, F. Aussenac, R. T. Weber, O. Ouari and P. Tordo, Highly Efficient, Water-Soluble Polarizing Agents for Dynamic Nuclear Polarization at High Frequency, *Angew. Chem., Int. Ed.*, 2013, **52**, 10858–10861.

33 C. Sauvée, G. Casano, S. Abel, A. Rockenbauer, D. Akhmetzyanov, H. Karoui, D. Siri, F. Aussenac, W. Maas, R. T. Weber, T. Prisner, M. Rosay, P. Tordo and O. Ouari, Tailoring of Polarizing Agents in the bTurea Series for Cross-Effect Dynamic Nuclear Polarization in Aqueous Media, *Chem.–Eur. J.*, 2016, **22**, 5598–5606.

34 G. Mathies, M. A. Caporini, V. K. Michaelis, Y. Liu, K.-N. Hu, D. Mance, J. L. Zweier, M. Rosay, M. Baldus and R. G. Griffin, Efficient Dynamic Nuclear Polarization at 800 MHz$\slash$527 GHz with Trityl-Nitroxide Biradicals, *Angew. Chem., Int. Ed.*, 2015, **54**, 11770–11774.

35 D. J. Kubicki, G. Casano, M. Schwarzwälder, S. Abel, C. Sauvée, K. Ganesan, M. Yulikov, A. J. Rossini, G. Jeschke, C. Copéret, A. Lesage, P. Tordo, O. Ouari and L. Emsley, Rational design of dinitroxide biradicals for efficient cross-effect dynamic nuclear polarization, *Chem. Sci.*, 2016, **7**, 550–558.

36 A. P. Jagtap, M.-A. Geiger, D. Stöppler, M. Orwick-Rydmark, H. Oschkinat and S. T. Sigurdsson, bcTol: a highly water-soluble biradical for efficient dynamic nuclear polarization of biomolecules, *Chem. Commun.*, 2016, **52**, 7020–7023.

37 S. Pylaeva, K. L. Ivanov, M. Baldus, D. Sebastiani and H. Elgabarty, Molecular Mechanism of Overhauser Dynamic Nuclear Polarization in Insulating Solids, *J. Phys. Chem. Lett.*, 2017, **8**, 2137–2142.

38 S. Bothe, J. Nowag, V. Klimavičius, M. Hoffmann, T. I. Troitskaya, E. V. Amosov, V. M. Tormyshev, I. Kirilyuk, A. Taratayko, A. Kuzhelev, D. Parkhomenko, E. Bagryanskaya, T. Gutmann and G. Buntkowsky, Novel Biradicals for Direct Excitation Highfield Dynamic Nuclear Polarization, *J. Phys. Chem. C*, 2018, **122**, 11422–11432.

39 F. Mentink-Vigier, I. Marin-Montesinos, A. P. Jagtap, T. Halbritter, J. van Tol, S. Hediger, D. Lee, S. T. Sigurdsson and G. De Paëpe, Computationally Assisted Design of Polarizing Agents for Dynamic Nuclear Polarization Enhanced NMR: The AsymPol Family, *J. Am. Chem. Soc.*, 2018, **140**, 11013–11019.

40 D. Wisser, G. Karthikeyan, A. Lund, G. Casano, H. Karoui, M. Yulikov, G. Menzildjian, A. C. Pinon, A. Purea, F. Engelke, S. R. Chaudhari, D. Kubicki, A. J. Rossini, I. B. Moroz, D. Gajan, C. Copéret, G. Jeschke, M. Lelli, L. Emsley, A. Lesage and O. Ouari, BDPA-Nitroxide Biradicals Tailored for Efficient Dynamic Nuclear Polarization Enhanced Solid-State NMR at Magnetic Fields up to 21.1 T, *J. Am. Chem. Soc.*, 2018, **140**, 13340–13349.

41 B. Corzilius, Paramagnetic Metal Ions for Dynamic Nuclear Polarization, in *eMagRes*, John Wiley & Sons, Ltd, 2018, pp. 179–194.

42 K. Sato, R. Hirao, I. Timofeev, O. Krumkacheva, E. Zaytseva, O. Rogozhnikova, V. M. Tormyshev, D. Trukhin, E. Bagryanskaya, T. Gutmann, C. Klimavicius, G. Buntkowsky, K. Sugisaki, S. Nakazawa, H. Matsuoka, K. Toyota, D. Shiomi and T. Takui, Trityl-Aryl-Nitroxide-Based Genuinely g-Engineered Biradicals, As Studied by Dynamic Nuclear Polarization, Multifrequency ESR/ENDOR, Arbitrary Wave Generator Pulse Microwave Waveform Spectroscopy, and Quantum Chemical Calculations, *J. Phys. Chem. A*, 2019, **123**, 7507–7517.

43 G. Stevanato, D. J. Kubicki, G. Menzildjian, A.-S. Chauvin, K. Keller, M. Yulikov, G. Jeschke, M. Mazzanti and L. Emsley, A Factor Two Improvement in High-Field Dynamic Nuclear Polarization from Gd(III) Complexes by Design, *J. Am. Chem. Soc.*, 2019, **141**, 8746–8751.

44 W. Zhai, A. Lucini Paioni, X. Cai, S. Narasimhan, J. Medeiros-Silva, W. Zhang, A. Rockenbauer, M. Weingarth, Y. Song, M. Baldus and Y. Liu, Postmodification *via* Thiol-Click Chemistry Yields Hydrophilic Trityl-Nitroxide Biradicals for Biomolecular High-Field Dynamic Nuclear Polarization, *J. Phys. Chem. B*, 2020, **124**, 9047–9060.

45 G. Stevanato, G. Casano, D. J. Kubicki, Y. Rao, L. Esteban Hofer, G. Menzildjian, H. Karoui, D. Siri, M. Cordova, M. Yulikov, G. Jeschke, M. Lelli, A. Lesage, O. Ouari and L. Emsley, Open and Closed Radicals: Local Geometry around Unpaired Electrons Governs Magic-Angle Spinning Dynamic Nuclear Polarization Performance, *J. Am. Chem. Soc.*, 2020, **142**, 16587–16599.

46 A. Lund, G. Casano, G. Menzildjian, M. Kaushik, G. Stevanato, M. Yulikov, R. Jabbour, D. Wisser, M. Renom-Carrasco, C. Thieuleux, F. Bernada, H. Karoui, D. Siri, M. Rosay, I. V. Sergeyev, D. Gajan, M. Lelli, L. Emsley, O. Ouari and A. Lesage, TinyPols: a family of water-soluble binitroxides tailored for dynamic nuclear polarization enhanced NMR spectroscopy at 18.8 and 21.1 T, *Chem. Sci.*, 2020, **11**, 2810–2818.

47 X. Cai, A. Lucini Paioni, A. Adler, R. Yao, W. Zhang, D. Beriashvili, A. Safeer, A. Gurinov, A. Rockenbauer, Y. Song, M. Baldus and Y. Liu, Highly Efficient Trityl-Nitroxide Biradicals for Biomolecular High-Field Dynamic Nuclear Polarization, *Chem.–Eur. J.*, 2021, **27**, 12758–12762.

48 A. Gurinov, B. Sieland, A. Kuzhelev, H. Elgabarty, T. D. Kühne, T. Prisner, J. Paradies, M. Baldus, K. L. Ivanov and S. Pylaeva, Mixed-Valence Compounds as Polarizing Agents for Overhauser Dynamic Nuclear Polarization in Solids, *Angew. Chem., Int. Ed.*, 2021, **60**, 15371–15375.

49 Y. Rao, C. T. Palumbo, A. Venkatesh, M. Keener, G. Stevanato, A. S. Chauvin, G. Menzildjian, S. Kuzin, M. Yulikov, G. Jeschke, A. Lesage, M. Mazzanti and L. Emsley, Design Principles for the Development of Gd(III) Polarizing Agents for Magic Angle Spinning Dynamic Nuclear Polarization, *J. Phys. Chem. C*, 2022, **126**, 11310–11317.

50 R. Harrabi, T. Halbritter, F. Aussenac, O. Dakhlaoui, J. van Tol, K. Damodaran, D. Lee, S. Paul, S. Hediger, F. Mentink-Vigier, S. Sigurdsson and G. De Paepe, Highly Efficient Polarizing Agents for MAS-DNP of Proton-dense Molecular Solids, *Angew. Chem., Int. Ed.*, 2022, **61**, e202114103.

51 T. Halbritter, R. Harrabi, S. Paul, J. van Tol, D. Lee, S. Hediger, S. T. Sigurdsson, F. Mentink-Vigier and G. De Paepe, PyrroTriPol: a semi-rigid trityl-nitroxide for high field dynamic nuclear polarization, *Chem. Sci.*, 2023, **14**, 3852–3864.

52 A. Venkatesh, G. Casano, Y. Rao, F. De Biasi, F. A. Perras, D. J. Kubicki, D. Siri, S. Abel, H. Karoui, M. Yulikov, O. Ouari and L. Emsley, Deuterated TEKPol Biradicals and the Spin-Diffusion Barrier in MAS DNP, *Angew. Chem., Int. Ed.*, 2023, **62**, e202304844.

53 G. Menzildjian, J. Schlagnitweit, G. Casano, O. Ouari, D. Gajan and A. Lesage, Polarizing agents for efficient high field DNP solid-state NMR spectroscopy under magic-angle spinning: from design principles to formulation strategies, *Chem. Sci.*, 2023, 6120–6148.

54 R. Harrabi, T. Halbritter, S. Alarab, S. Chatterjee, M. Wolska-Pietkiewicz, K. K. Damodaran, J. van Tol, D. Lee, S. Paul, S. Hediger, S. T. Sigurdsson, F. Mentink-Vigier and G. De Paëpe, AsymPol-TEKs as efficient polarizing agents for MAS-DNP in glass matrices of non-aqueous solvents, *Phys. Chem. Chem. Phys.*, 2024, **26**, 5669–5682.

55 A. V. Kessenikh and A. A. Manenkov, Dynamic Polarization of Nuclei During Saturation of Nonuniformly Broadened Electron Paramagnetic Resonance Lines, *Soviet Physics – Solid State*, 1963, **5**, 835–837.

56 C. F. Hwang and D. A. Hill, Phenomenological Model for the New Effect in Dynamic Polarization, *Phys. Rev. Lett.*, 1967, **19**, 1011–1014.

57 T. Maly, G. T. Debelouchina, V. S. Bajaj, K.-N. Hu, C.-G. Joo, M. L. Mak-Jurkauskas, J. R. Sirigiri, P. C. A. van der Wel, J. Herzfeld, R. J. Temkin and R. G. Griffin, Dynamic nuclear polarization at high magnetic fields, *J. Chem. Phys.*, 2008, **128**, 052211.

58 K. R. Thurber and R. Tycko, Theory for cross effect dynamic nuclear polarization under magic-angle spinning in solid state nuclear magnetic resonance: the importance of level crossings, *J. Chem. Phys.*, 2012, **137**, 084508.

59 Y. Hovav, A. Feintuch and S. Vega, Theoretical aspects of dynamic nuclear polarization in the solid state – The cross effect, *J. Magn. Reson.*, 2012, **214**, 29–41.

60 F. Mentink-Vigier, U. Akbey, H. Oschkinat, S. Vega and A. Feintuch, Theoretical aspects of Magic Angle Spinning – Dynamic Nuclear Polarization, *J. Magn. Reson.*, 2015, **258**, 102–120.

61 D. Mance, P. Gast, M. Huber, M. Baldus and K. L. Ivanov, The magnetic field dependence of cross-effect dynamic nuclear polarization under magic angle spinning, *J. Chem. Phys.*, 2015, **142**, 234201.

62 A. Purea, C. Reiter, A. I. Dimitriadis, E. d. Rijk, F. Aussenac, I. Sergeyev, M. Rosay and F. Engelke, Improved waveguide coupling for 1.3 mm MAS DNP probes at 263 GHz, *J. Magn. Reson.*, 2019, **302**, 43–49.

63 A. J. Rossini, A. Zagdoun, M. Lelli, D. Gajan, F. Rascon, M. Rosay, W. E. Maas, C. Coperet, A. Lesage and L. Emsley, One hundred fold overall sensitivity enhancements for Silicon-29 NMR spectroscopy of surfaces by dynamic nuclear polarization with CPMG acquisition, *Chem. Sci.*, 2012, **3**, 108–115.

64 H. Takahashi, S. Hediger and G. De Paepe, Matrix-free dynamic nuclear polarization enables solid-state NMR 13C–13C correlation spectroscopy of proteins at natural isotopic abundance, *Chem. Commun.*, 2013, **49**, 9479–9481.

65 F. Mentink-Vigier, S. Paul, D. Lee, A. Feintuch, S. Hediger, S. Vega and G. De Paëpe, Nuclear depolarization and absolute sensitivity in magic-angle spinning cross effect dynamic nuclear polarization, *Phys. Chem. Chem. Phys.*, 2015, **17**, 21824–21836.

66 F. A. Perras, A. Sadow and M. Pruski, *In Silico* Design of DNP Polarizing Agents: Can Current Dinitroxides Be Improved?, *ChemPhysChem*, 2017, **18**, 2279–2287.

67 F. Mentink-Vigier, S. Vega and G. De Paëpe, Fast and accurate MAS–DNP simulations of large spin ensembles, *Phys. Chem. Chem. Phys.*, 2017, **19**, 3506–3522.

68 F. Mentink-Vigier, A.-L. Barra, J. van Tol, S. Hediger, D. Lee and G. De Paëpe, De novo prediction of cross-effect efficiency for magic angle spinning dynamic nuclear polarization, *Phys. Chem. Chem. Phys.*, 2019, **21**, 2166–2176.

69 F. Mentink-Vigier, Optimizing nitroxide biradicals for cross-effect MAS-DNP: the role of g-tensors' distance, *Phys. Chem. Chem. Phys.*, 2020, **22**, 3643–3652.

70 F. Mentink-Vigier, T. Dubroca, J. V. Tol and S. T. Sigurdsson, The distance between g-tensors of nitroxide biradicals governs MAS-DNP performance: the case of the bTurea family, *J. Magn. Reson.*, 2021, **329**, 107026.

71 A. Venkatesh, G. Casano, R. Wei, Y. Rao, H. Lingua, H. Karoui, M. Yulikov, O. Ouari and L. Emsley, Rational Design of Dinitroxide Polarizing Agents for Dynamic Nuclear Polarization to Enhance Overall NMR Sensitivity, *Angew. Chem., Int. Ed.*, 2024, e202317337.

72 K. R. Thurber and R. Tycko, Perturbation of nuclear spin polarizations in solid state NMR of nitroxide-doped samples by magic-angle spinning without microwaves, *J. Chem. Phys.*, 2014, **140**, 184201.

73 S. Hediger, D. Lee, F. Mentink-Vigier and G. De Paëpe, MAS-DNP Enhancements: Hyperpolarization, Depolarization, and Absolute Sensitivity, in *eMagRes*, John Wiley & Sons, Ltd, 2018, pp. 105–116.

74 S. R. Chaudhari, P. Berruyer, D. Gajan, C. Reiter, F. Engelke, D. L. Silverio, C. Copéret, M. Lelli, A. Lesage and L. Emsley, Dynamic nuclear polarization at 40 kHz magic angle spinning, *Phys. Chem. Chem. Phys.*, 2016, **18**, 10616–10622.

75 P. Berruyer, S. Björgvinsdóttir, A. Bertarello, G. Stevanato, Y. Rao, G. Karthikeyan, G. Casano, O. Ouari, M. Lelli, C. Reiter, F. Engelke and L. Emsley, Dynamic Nuclear Polarization Enhancement of 200 at 21.15 T Enabled by 65 kHz Magic Angle Spinning, *J. Phys. Chem. Lett.*, 2020, **11**, 8386–8391.

76 S. Stoll and A. Schweiger, EasySpin, a comprehensive software package for spectral simulation and analysis in EPR, *J. Magn. Reson.*, 2006, **178**, 42–55.

77 N. A. Prisco, A. C. Pinon, L. Emsley and B. F. Chmelka, Scaling analyses for hyperpolarization transfer across a spin-diffusion barrier and into bulk solid media, *Phys. Chem. Chem. Phys.*, 2021, **23**, 1006–1020.

78 F. A. Perras, M. Raju, S. L. Carnahan, D. Akbarian, A. C. T. van Duin, A. J. Rossini and M. Pruski, Full-Scale *Ab Initio* Simulation of Magic-Angle-Spinning Dynamic Nuclear Polarization, *J. Phys. Chem. Lett.*, 2020, **11**, 5655–5660.

79 F. Mentink-Vigier, Optimizing nitroxide biradicals for cross-effect MAS-DNP: the role of g-tensors' distance, *Phys. Chem. Chem. Phys.*, 2020, **22**, 3643–3652.

80 M. Mardini, R. S. Palani, I. M. Ahmad, S. Mandal, S. K. Jawla, E. Bryerton, R. J. Temkin, S. T. Sigurdsson and R. G. Griffin, Frequency-swept dynamic nuclear polarization, *J. Magn. Reson.*, 2023, **353**, 107511.

81 A. Volkov, C. Dockter, T. Bund, H. Paulsen and G. Jeschke, Pulsed EPR Determination of Water Accessibility to Spin-Labeled Amino Acid Residues in LHCIIb, *Biophys. J.*, 2009, **96**, 1124–1141.

82 K. O. Tan, M. Mardini, C. Yang, J. H. Ardenkjær-Larsen and R. G. Griffin, Three-spin solid effect and the spin diffusion barrier in amorphous solids, *Sci. Adv.*, 2019, **5**, eaax2743.

83 F. Hecker, L. Fries, M. Hiller, M. Chiesa and M. Bennati, O-17 Hyperfine Spectroscopy Reveals Hydration Structure of Nitroxide Radicals in Aqueous Solutions, *Angew. Chem., Int. Ed.*, 2022, **62**, e202213700.

84 E. R. Canarie, S. M. Jahn and S. Stoll, Quantitative Structure-Based Prediction of Electron Spin Decoherence in Organic Radicals, *J. Phys. Chem. Lett.*, 2020, **11**, 3396–3400.

85 A. A. Smith, B. Corzilius, A. B. Barnes, T. Maly and R. G. Griffin, Solid effect dynamic nuclear polarization and polarization pathways, *J. Chem. Phys.*, 2012, **136**, 015101.
86 A. C. Pinon, J. Schlagnitweit, P. Berruyer, A. J. Rossini, M. Lelli, E. Socie, M. Tang, T. Pham, A. Lesage, S. Schantz and L. Emsley, Measuring Nano- to Microstructures from Relayed Dynamic Nuclear Polarization NMR, *J. Phys. Chem. C*, 2017, **121**, 15993–16005.
87 S. Chatterjee, A. Venkatesh, S. T. Sigurdsson and F. Mentink-Vigier, Role of Protons in and around Strongly Coupled Nitroxide Biradicals for Cross-Effect Dynamic Nuclear Polarization, *J. Phys. Chem. Lett.*, 2024, 2160–2168.
88 F. J. Scott, T. Dubroca, R. W. Schurko, S. Hill, J. R. Long and F. Mentink-Vigier, Characterization of dielectric properties and their impact on MAS-DNP NMR applications, *J. Magn. Reson.*, 2024, **365**, 107742.
89 G. J. Li, B. Dastrup, R. S. Palani, M. A. Shapiro, S. K. Jawla, R. G. Griffin, K. A. Nelson and R. J. Temkin, Design and optimization of THz coupling in zirconia MAS rotors for dynamic nuclear polarization NMR, *J. Magn. Reson.*, 2024, **364**, 107722.